Optical signatures of suppressed carrier localization in encapsulated WSe$_2$ monolayer

Raqibul Hossen ; Sang-Hyuk Park; Seong-Yeon Lee; Ki-Ju Yee; Sang-Youp Yim ✉ ; Young-Dahl Jho ✉

Check for updates

CrossMark

View Online

Export Citation

Articles You May Be Interested In

Observation of split defect-bound excitons in twisted WSe$_2$/WSe$_2$ homostructure

Appl. Phys. Lett. (October 2020)

Elastic properties of suspended multilayer WSe$_2$

Appl. Phys. Lett. (January 2016)

Photoresponse of homostructure WSe$_2$ rectifying diode

AIP Advances (July 2019)

Optical signatures of suppressed carrier localization in encapsulated WSe$_2$ monolayer

View Online   Export Citation   CrossMark

Raqibul Hossen,[1,2] (ID) Sang-Hyuk Park,[3] Seong-Yeon Lee,[4] Ki-Ju Yee,[4] Sang-Youp Yim,[2,a] (ID) and Young-Dahl Jho[1,a] (ID)

AFFILIATIONS

[1] School of Electrical Engineering and Computer Science, Gwangju Institute of Science and Technology, Gwangju 61005, South Korea
[2] Advanced Photonics Research Institute (APRI), Gwangju Institute of Science and Technology, Gwangju 61005, South Korea
[3] Clarendon Laboratory, Department of Physics, University of Oxford, Oxford OX1 3PU, United Kingdom
[4] Department of Physics, Chungnam National University, Daejeon 34134, South Korea

[a] Authors to whom correspondence should be addressed: jho@gist.ac.kr and syim@gist.ac.kr

ABSTRACT

Low carrier mobility, closely associated with the formation of localized states, is the major bottleneck of utilizing the unique quantum transport properties in transition metal dichalcogenides (TMDCs). Here, we demonstrate an effective method to quantify the localization energy based on the temperature-dependent spectral variation of photoluminescence (PL) in pristine and hexagonal boron nitride (h-BN) encapsulated monolayer (ML) WSe$_2$. Considering the protecting capability of h-BN against contamination and degradation, while not affecting the electronic structure as an insulating dielectric, the localization energy was comparatively extracted out of PL spectra in pristine and encapsulated ML WSe$_2$. In pristine ML WSe$_2$, two distinctive energy traces were resolved with an energy difference of about 17 meV, which was associated with the localized state revealed below 200 K. Clear evidence for the carrier localization was also evident in the integrated PL intensity trace with temperature as the trace from pristine ML clearly deviates from the dark-exciton-like behavior of ML WSe$_2$, violating the spin selection rule of the lowest exciton state. In clear contrast, the temperature dependency of the h-BN encapsulated ML WSe$_2$ in PL spectra matches well with the typical Varshni formula of free excitonic peaks and the integrated intensity trace of thermally populated spin subbands. Our study suggests that the h-BN encapsulation could suppress the carrier localization channels by avoiding surface oxidation due to air exposure and could provide insights into how one could preserve the excitonic features in TMDC materials and devices.

The emergence of numerous exciton-related properties in the monolayer (ML) transition metal dichalcogenides (TMDCs) has inspired its potential pragmatic devices, as their electronic and optical features are precisely controllable. The inherent inversion symmetry lacking along with spin-valley coupling in the ML TMDCs[1] consequence in various interesting quantum-transport phenomena, such as current-induced spin accumulation[2] and valley Hall effect.[3,4] Concomitantly, the different spin configurations at ±K valleys in the ML TMDCs lead to the valley-specific optical selection rules[5,6] so that the interband transition at each valley is coupled to different circularly polarized lights.[7] Modification of the crystalline properties, induced by strain, defects, and encapsulation, could further affect the band-edge emission features.[7,8]

Analysis of the optical properties regarding excitonic complexes has been feasible due to strong Coulomb interaction in ML TMDCs.[9] Although complex excitonic characteristics often disclosed significant discrepancies in the optical measurements, e.g., binding energy values ranging between 198 and 790 meV;[9–11] furthermore, transport investigations have revealed low carrier mobility[12,13] possibly due to high impurities and corresponding localization channels. Remarkably, the large surface area-to-volume ratio of ML TMDCs compared to the bulk crystals makes them more susceptible to impurities in the adjacent dielectric environment; e.g., when dealing with pristine TMDCs, charged impurities in the substrate influence their transport properties.[14–16] In this respect, In this regard, we note that experimental exploration of the various

mechanisms associated with localization in TMDCs is still lacking, including impurity-related localization, localization-dependent band-edge emission traits, and scattering between various carriers in the vicinity of localization traps.

Photoluminescence (PL) has been successfully correlated with the transport properties encompassing localization traps in various materials, such as semiconductors,[17] organic materials,[18] and carbon derivatives.[19] Although there have been several reports on the temperature-dependent PL properties of TMDCs,[9,11,20–22] they have mainly focused on the complex fine structures of charged exciton states.[23] Although the localization features were revealed through the results of these low-temperature experiments,[24,25] the quantification of the localization energy and the change in properties due to the environmental perturbations inherent in the heterostructures have not been addressed. Representatively, the characterization of suppressed carrier localization in encapsulated samples relative to pristine counterparts has never been investigated. In particular, since the localized state is not affected by the valley-spin coupling, which determines the excitonic emission characteristics,[9] it is important to verify whether the PL signal follows the optical selection rules of the band edge.[26] In this work, we quantified the localization energy in pristine ML WSe_2 and demonstrated carrier localization suppression due to h-BN encapsulation using a comparative PL spectral analysis as a function of temperature.

An h-BN encapsulated WSe_2 ML was attained by chronologically transferring a bottom h-BN flake, ML WSe_2, and top h-BN flake exfoliated mechanically from bulk crystals with adhesive tape onto a quartz substrate.[27] The pristine and h-BN-encapsulated ML flakes are visible in Fig. 1(a) as an optical micrograph of the sample, where the colored lines define the boundary of the bottom h-BN (green), WSe_2 ML (yellow) and top h-BN (light-green) with an average thickness of 30, 1.1, and 5 nm correspondingly, an inset schematic visualizes the vertical distribution of the layers.

Raman measurements were performed in backscattering geometry using a LabRam HR spectrometer (Horiba) with a 532 nm CW laser (Torus 532), at roo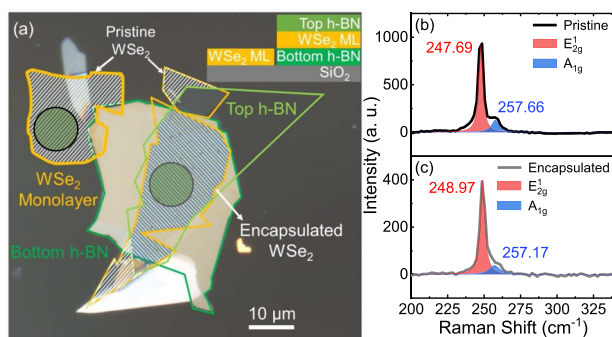m temperature, with a spectral range of 200–2200 and 1 cm^{-1} resolution utilizing a grating of 600 gr/mm while measuring. A Raman map encompassing both pristine and encapsulated regions was obtained by the 57 × 57 point scans with a total dwell time of 0.84 s per point. The laser beam was focused by 100× objectives with a numerical aperture (N.A.) of 0.95, at 0.5 mW. Time-integrated PL (TIPL) was measured utilizing a micro PL setup by exciting the sample with a 532 nm CW laser (LVI532-30-LN), at 50 μW. A 20× objective lens (0.2 N.A.) was utilized to focus the excitation beam with a spot size of around ~10 μm on the sample, as well as to collect PL signals. We selectively chose spots with fewer bubbles while exciting the encapsulated portion to minimize the bubble-related strain-induced PL signature. The collected signal was directed to a 1200 gr/mm grating of a spectrometer (SpectraPro-2300) equipped with a monochromator attached to a nitrogen-cooled charge-coupled device with 0.14 nm of resolution and a PMT resolution of 0.1 nm, while the temperature was varied from 77 to 295 K using a liquid nitrogen cryostat (Janis ST-500).

We characterized the ML nature and vibrational properties of both pristine and encapsulated WSe_2 using Raman mapping at room temperature. Extracted spectra from Raman map for pristine (h-BN encapsulated) WSe_2 ML shown in Figs. 1(b) and 1(c) depict two prominent peaks, E_{2g}^1 (in-plane mode) at 247.69 cm^{-1} (248.97 cm^{-1}) and A_{1g} (out-of-plane mode) at 257.66 cm^{-1} (257.11 cm^{-1}).[28] To avoid the strain effect associated with bubbles extraction points in the encapsulated portion were intentionally selected to avoid bubbles. E_{2g}^1 (A_{1g}) peak of air exposed WSe_2 blueshifts (redshifts) by 1.28 cm^{-1} (0.49 cm^{-1}) from that of h-BN encapsulated WSe_2 ML, likely due to defect creation[29] or strain[30] introduced during oxidation or dielectric surrounding variation, respectively. As in our sample no splitting of the E_{2g}^1 peak has been observed, we can attribute the observed Raman frequency blue-shift in air-exposed WSe_2 ML to hole-doping, induced by the oxygen adsorption in ambient condition.[31]

Figures 2(a) and 2(b) show a direct comparison of the temperature evolution of TIPL spectra from (a) pristine and (b) h-BN encapsulated area. Below 175 K two peaks were clearly visible, where the PL spectra obtained from the pristine (h-BN encapsulated) ML WSe_2 at 77 K peaks observed at 1.693 eV (1.688 eV) was associated with the neutral exciton (X^0) while the other peak detected at 1.658 eV (1.652 eV) was linked to the trion (X^-) emission, giving an X^- binding energy of 35 meV (36 meV), a few meV higher than the X^- binding energy value ~30 meV of ML WSe_2.[11] When the temperature was increased the X^0 peak dominates the PL spectrum with a prolonged low-energy tail, indicating the existence of X^- at ambient temperature. A solo peak at 1.64 eV (1.63 eV) seen from the pristine (h-BN encapsulated) portion at room temperature, associated with the lowest energy exciton state with no lower energy indirect gap emission characteristics, confirms the ML nature of the sample.[6,9] The colored line in Figs. 2(a) and 2(b), guides the eye to the redshift induced by the temperature-dependent band-structure change. Notably, the PL linewidth sharpens substantially with h-BN encapsulation, and the X^0 energy of the pristine WSe_2 is 25.9 meV higher than that of the encapsulated WSe_2, we ascribe these effects to the influence of environmental factors on exciton binding energies.[27,32] To quantify the localization energy, we analyzed the energy evolution of the X^0 PL peak with temperature.

FIG. 1. (a) Optical micrograph showing ML pristine and h-BN encapsulated WSe_2, with colored lines showing boundaries of bottom h-BN (green), WSe_2 ML (yellow) and top h-BN (light-green), additionally beam position indicated by a green shaded circle. Raman spectra of pristine and encapsulated portions extracted from the Raman map are shown in (b) and (c), with red and blue shaded lines representing Lorentzian fitting peaks corresponding to (E_{2g}^1 and A_{1g}) Raman modes in ML WSe_2.
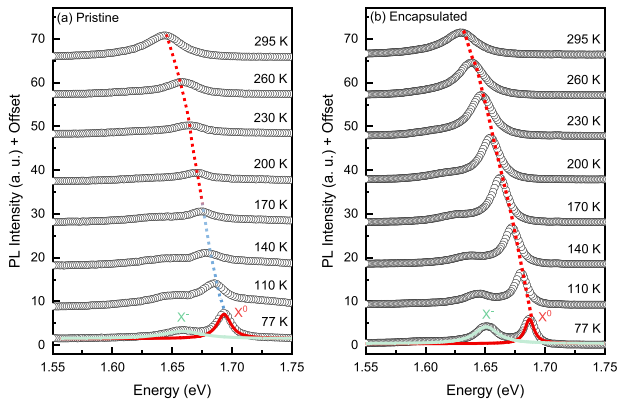
FIG. 2. Temperature evolution of the normalized PL spectra obtained from (a) pristine and (b) encapsulated ML WSe$_2$. For convenience, the spectra at different temperatures were shifted vertically and a colored guiding line depicts the neutral exciton (X^0) emission signature. The photoluminescence spectrum at the lowest measuring temperature in the pristine (encapsulated) case has been decomposed into two Lorentzian peaks shown in light green and red lines.

Figure 3 depicts the temperature dependency of the PL peak energy in (a) pristine and (b) h-BN encapsulated WSe$_2$ ML under identical conditions, where the energy values were extracted by fitting the peaks with a Lorentz function, considering the homogeneity of the luminescence from ML TMDCs.[10] Noticeably in both cases, the

exciton energies undergo a red shift with increasing temperature, which is a typical property of semiconductors, and can be well fitted by the relations describing bandgap evolution with temperature like Varshni model described as[33] $E(T) = E_0 - \alpha T^2/(\beta + T)$, where E_0 is the bandgap at 0 K, and α and β are the weighting factors associated with the temperature-dependent lattice dilatation and average phonon temperature, respectively. From fitting, we obtained $\alpha = 4.2 \times 10^{-4}$ eV/K in pristine and $\alpha = 3.7 \times 10^{-4}$ eV/K in encapsulated case, while the average phonon temperature of 170 K for both, consistent with the values reported previously.[34,35]

In pristine ML WSe$_2$, the X^0 peak energy shift shows a notable deviation from the Varshni model at the lower temperature range, while in the encapsulated ML WSe$_2$ that exactly follows the model. Such temperature-dependent initial blue shift and subsequent red shift of the emission peak energy was revealed in various semiconductor systems,[36,37] including TMDCs,[24,38] which was associated with thermal redistribution of excitons inside localization centers with a mean energy of $E_{\Delta loc}$.[39] So, we fitted the lower temperature peak energy values separately, gray line in Fig. 3(a), and extracted the localization energy as 17.4 meV from the energy difference of the fitted curves. The slope change disappears above 200 K, implying carrier delocalization. In contrast, the Varshni fit was consistent with the experimental results in encased WSe$_2$, implying that encapsulation minimized defect-induced carrier localization. The error bar in Figs. 3(a) and 3(b) is showing the PL linewidth, which increases gradually with increasing temperature in the lower temperature range (<175 K), and then increases rapidly from 200 to 300 K. The increased exciton–phonon interaction at high temperatures, as well as the activation of nonradiative recombination centers, contribute
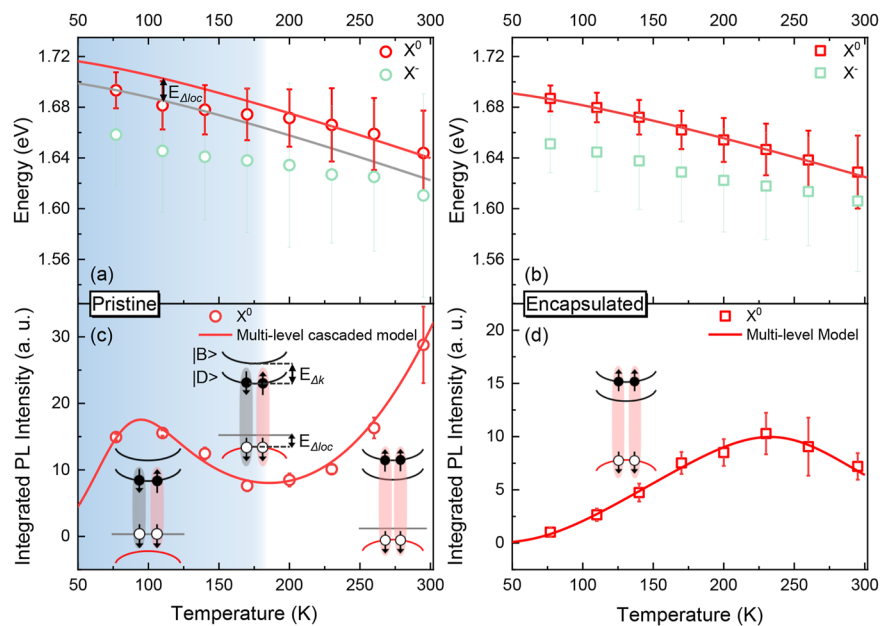
FIG. 3. Temperature evolution of PL peak energy in (a) pristine and (b) h-BN encapsulated WSe$_2$ ML, with red scatters showing measured data, error bars indicating linewidth, and red solid lines representing fitted data using Varshni's model. Temperature assessment of the extracted integrated intensity from (c) pristine and (d) h-BN encapsulated WSe$_2$ ML, where red scatters are the measured values, while the red line shows the fitting data using the multi-level cascaded (multi-level) model.

to the accelerated broadening of the PL peak. Observed carrier localization in the pristine portion is likely to be induced from oxygen defects, created due to the oxidation and adsorption at the surface upon air exposure, while in encapsulated ML carrier localization is suppressed by minimizing chemical reactions at the ML surface with ambient oxygen.[40] The asymmetricity of the PL spectrum at low temperatures is more prominent in the pristine than that of the encapsulated ML WSe$_2$, which was attributed to the hole localization. Moreover, instead of chalcogen vacancies, tungsten vacancies in WSe$_2$, which induce trap states within the bandgap near valence band maxima, are more dominant due to oxidation, as resultant WO$_x$ acts as a strong hole injection layer.[41,42]

In order to better comprehend the strong exciton behavior and reveal the exciton binding energies in WSe$_2$ ML, we investigated the temperature evolution of the PL integrated intensity. By using the Lorentzian fitting function to fit the emission peaks in Fig. 2, we were able to extract the integrated PL intensities, which are represented by red circles (squares) for the pristine (encapsulated) WSe$_2$ ML in Figs. 3(c) and 3(d). Integrated PL intensity obtained from the pristine WSe$_2$ ML decreases with rising temperature up to 175 K before increasing in pristine WSe$_2$ ML, as shown in Fig. 3(c). The initial higher intensity in the lowest temperature can be ascribed to the easier thermalization of the localized states, hence the radiative recombination of trapped carriers. Additional thermalization of these localized carriers causes them to delocalize into the spin-forbidden dark $|D\rangle_{SF}$ state; hence, a monotonic decrease of the integrated intensity with increasing temperature was anticipated. Above 175 K, we observe the bright excitonic behavior where the electrons thermalized to bright $|B\rangle$ states from the $|D\rangle_{SF}$ state; thus, PL intensity increases with increasing temperature. This sequential drop and rise have been fitted by the cascaded multi-level model defined by[11,43–45]

$$I(T) = I_1(0)\frac{1 + Ae^{-E_{\Delta k}/k_B T}}{1 + Be^{-E_b/k_B T}} + I_2(0)\frac{1}{1 + Ce^{-E_{\Delta loc}/k_B T}}, \quad (1)$$

where $I_1(0)$ and $I_2(0)$ are the PL intensity at 0 K for the neutral and localized excitonic emission, respectively, A, B, and C are amplitude weighting factors, and $E_{\Delta loc}$, $E_{\Delta k}$, and E_b correspond to the activation energy for the transition from localized states, bright state, free excitonic state, respectively, which defines the sequential decrease and increase in PL intensity. From the fitting, solid red line in Fig. 3(c), we attained the $E_{\Delta loc}$, $E_{\Delta k}$, and E_b to be 17, 38, and 239 meV, respectively. Notably, these values are comparable to the localization energy (17 meV) calculated from Fig. 3(a), dark and bright excitonic band separation in WSe$_2$ (40 meV)[8] and exciton binding energy (198 meV)[11] reported earlier.

Contrarily, the integrated PL intensity trace from encapsulated WSe$_2$ ML shows only delocalized emission, as shown in Fig. 3(d). The increase in the integrated intensity was due to the radiative recombination from $|B\rangle$ state at lower temperatures and can be fitted well with the multi-level model described by[11,43–45]

$$I(T) = I_1(0)\frac{1 + Ae^{-E_{\Delta k}/k_B T}}{1 + Be^{-E_b/k_B T}}, \quad (2)$$

where $I_1(0)$ is the PL intensity at 0 K, A and B as amplitude weighting factors, $E_{\Delta k}$ corresponds to the dark and bright excitonic band separation energy, while E_b corresponds to the exciton binding energy. From the fitting, we obtained E_b = 201 meV, which is analogous to the previously reported value of 198 meV[11] and $E_{\Delta k}$ = 26 meV. Furthermore, the signatures of the momentum forbidden dark $(|D\rangle_{MF})$ states have been revealed in the high-temperature range, supporting the theoretical prediction.[46] Notably, both $E_{\Delta k}$ and E_b values extracted from fitting are lower in the encapsulated case than the pristine, which can be ascribed to the improved e-h wavefunction spatial overlap and change in relative permittivity of adjacent dielectric (ε_{avg}). As in h-BN encapsulated WSe$_2$ ML ε_{avg} (6.9) is much larger than that of the pristine WSe$_2$ ML (2.3), the electronic bandgap and the binding energies of exciton complexes decrease substantially.[32]

In summary, we have investigated the localization characteristics of both pristine and h-BN encapsulated ML WSe$_2$ by using temperature-dependent TIPL. We have observed two distinct emission peaks in the PL spectra of the pristine sample, which we attribute to the existence of a localized state at lower energy than the neutral exciton. Clear evidence for these localized states was also evident in the integrated intensity trace as it clearly shows the localization and delocalization phenomena with temperature variation, while in the encapsulated WSe$_2$ ML, both energy and intensity trace confirm suppression of this localization phenomena. Hence, the localization characteristics of TMDCs in ambient conditions suggest the critical role of h-BN encapsulation as a protective strategy to preserve the excitonic properties in TMDC materials for their prospective use in functional devices.

AUTHOR DECLARATIONS

Conflict of Interest

The authors have no conflicts to disclose.

Author Contributions

Raqibul Hossen: Conceptualization (equal); Data curation (lead); Formal analysis (lead); Investigation (equal); Methodology (equal); Resources (supporting); Software (equal); Validation (equal); Visualization (equal); Writing – original draft (lead); Writing – review & editing (equal). **Sang-Hyuk Park**: Formal analysis (supporting); Methodology (supporting); Writing – review & editing (supporting). **Seong-Yeon Lee**: Data curation (equal); Formal analysis (supporting); Methodology (supporting); Writing – original draft (supporting); Writing – review & editing (supporting). **Ki-Ju Yee**: Conceptualization (supporting); Investigation (supporting); Methodology (supporting); Writing – review & editing (supporting). **Sang-Youp Yim**: Conceptualization (equal); Formal analysis (equal); Investigation (equal); Methodology (equal); Resources (equal); Supervision (supporting); Validation (supporting); Writing – original draft (supporting); Writing – review & editing (equal). **Young-Dahl Jho**: Conceptualization (lead); Data curation

(equal); Formal analysis (equal); Funding acquisition (lead); Investigation (lead); Methodology (equal); Project administration (lead); Resources (lead); Software (supporting); Supervision (lead); Validation (lead); Visualization (equal); Writing – original draft (lead); Writing – review & editing (lead).

DATA AVAILABILITY

The data that support the findings of this study are available from the corresponding author upon reasonable request.

REFERENCES

[1] T. Cao, G. Wang, W. Han, H. Ye, C. Zhu, J. Shi, Q. Niu, P. Tan, E. Wang, B. Liu, and J. Feng, Nat. Commun. **3**, 887 (2012).

[2] X. Qian, J. Liu, L. Fu, and J. Li, Science **346**, 1344–1347 (2014).

[3] K. F. Mak, K. L. McGill, J. Park, and P. L. McEuen, Science **344**, 1489–1492 (2014).

[4] J. Lee, K. F. Mak, and J. Shan, Nat. Nanotechnol. **11**, 421–425 (2016).

[5] K. F. Mak, K. He, J. Shan, and T. F. Heinz, Nat. Nanotechnol. **7**, 494–498 (2012).

[6] H. Zeng, G.-B. Liu, J. Dai, Y. Yan, B. Zhu, R. He, L. Xie, S. Xu, X. Chen, W. Yao, and X. Cui, Sci. Rep. **3**, 1608 (2013).

[7] X.-X. Zhang, T. Cao, Z. Lu, Y.-C. Lin, F. Zhang, Y. Wang, Z. Li, J. C. Hone, J. A. Robinson, D. Smirnov et al., Nat. Nanotechnol. **12**, 883–888 (2017).

[8] H.-Y. Hwang, S. Lee, Y.-H. Kim, F. Ullah, C. T. Le, Y. S. Kim, K.-J. Yee, C. J. Stanton, and Y.-D. Jho, 2D Mater. **9**, 015011 (2021).

[9] K. He, N. Kumar, L. Zhao, Z. Wang, K. F. Mak, H. Zhao, and J. Shan, Phys. Rev. Lett. **113**, 026803 (2014).

[10] A. T. Hanbicki, M. Currie, G. Kioseoglou, A. L. Friedman, and B. T. Jonker, Solid State Commun. **203**, 16–20 (2015).

[11] J. Huang, T. B. Hoang, and M. H. Mikkelsen, Sci. Rep. **6**, 22414 (2016).

[12] S. Ghatak, A. N. Pal, and A. Ghosh, ACS Nano **5**, 7707–7712 (2011).

[13] S. Ahmed and J. Yi, Nano-Micro Lett. **9**, 50 (2017).

[14] G.-H. Lee, X. Cui, Y. D. Kim, G. Arefe, X. Zhang, C.-H. Lee, F. Ye, K. Watanabe, T. Taniguchi, P. Kim, and J. Hone, ACS Nano **9**, 7019–7026 (2015).

[15] H. Yu, Z. Yang, L. Du, J. Zhang, J. Shi, W. Chen, P. Chen, M. Liao, J. Zhao, J. Meng et al., Small **13**, 1603005 (2017).

[16] Y. Uchiyama, A. Kutana, K. Watanabe, T. Taniguchi, K. Kojima, T. Endo, Y. Miyata, H. Shinohara, and R. Kitaura, npj 2D Mater. Appl. **3**, 26 (2019).

[17] R. L. Weiher and W. C. Tait, Phys. Rev. B **5**, 623 (1972).

[18] P. Irkhin and I. Biaggio, Phys. Rev. Lett. **107**, 017402 (2011).

[19] S. Moritsubo, T. Murai, T. Shimada, Y. Murakami, S. Chiashi, S. Maruyama, and Y. K. Kato, Phys. Rev. Lett. **104**, 247402 (2010).

[20] J. Jadczak, J. Kutrowska-Girzycka, P. Kapuściński, Y. S. Huang, A. Wójs, and L. Bryja, Nanotechnology **28**, 395702 (2017).

[21] E. V. Calman, L. H. Fowler-Gerace, D. J. Choksy, L. V. Butov, D. E. Nikonov, I. A. Young, S. Hu, A. Mishchenko, and A. K. Geim, Nano Lett. **20**, 1869–1875 (2020).

[22] C. Robert, S. Park, F. Cadiz, L. Lombez, L. Ren, H. Tornatzky, A. Rowe, D. Paget, F. Sirotti, M. Yang et al., Nat. Commun. **12**, 5455 (2021).

[23] A. Arora, N. K. Wessling, T. Deilmann, T. Reichenauer, P. Steeger, P. Kossacki, M. Potemski, S. M. de Vasconcellos, M. Rohlfing, and R. Bratschitsch, Phys. Rev. B **101**, 241413 (2020).

[24] T. Yan, X. Qiao, X. Liu, P. Tan, and X. Zhang, Appl. Phys. Lett. **105**, 101901 (2014).

[25] H. Masenda, L. M. Schneider, M. Adel Aly, S. J. Machchhar, A. Usman, K. Meerholz, F. Gebhard, S. D. Baranovskii, and M. Koch, Adv. Electron. Mater. **7**, 2100196 (2021).

[26] M. R. Molas, C. Faugeras, A. O. Slobodeniuk, K. Nogajewski, M. Bartos, D. M. Basko, and M. Potemski, 2D Mater. **4**, 021003 (2017).

[27] S.-Y. Lee, T.-Y. Jeong, S. Ahn, S. Jung, Y.-H. Cho, and K.-J. Yee, Nanomaterials **10**, 350 (2020).

[28] M. Yamamoto, S. Dutta, S. Aikawa, S. Nakaharai, K. Wakabayashi, M. S. Fuhrer, K. Ueno, and K. Tsukagoshi, Nano Lett. **15**, 2067–2073 (2015).

[29] T.-J. Ha, K. Chen, S. Chuang, K. M. Yu, D. Kiriya, and A. Javey, Nano Lett. **15**, 392–397 (2015).

[30] S. B. Desai, G. Seol, J. S. Kang, H. Fang, C. Battaglia, R. Kapadia, J. W. Ager, J. Guo, and A. Javey, Nano Lett. **14**, 4592–4597 (2014).

[31] M. Yamamoto, T. L. Einstein, M. S. Fuhrer, and W. G. Cullen, J. Phys. Chem. C **117**, 25643–25649 (2013).

[32] S. Borghardt, J.-S. Tu, F. Winkler, J. Schubert, W. Zander, K. Leosson, and B. E. Kardynał, Phys. Rev. Mater. **1**, 054001 (2017).

[33] Y. P. Varshni, Physica **34**, 149–154 (1967).

[34] A. Arora, M. Koperski, K. Nogajewski, J. Marcus, C. Faugeras, and M. Potemski, Nanoscale **7**, 10421–10429 (2015).

[35] P. Qi, Y. Luo, B. Shi, W. Li, D. Liu, L. Zheng, Z. Liu, Y. Hou, and Z. Fang, eLight **1**, 6 (2021).

[36] M. Kondow, S. Minagawa, Y. Inoue, T. Nishino, and Y. Hamakawa, Appl. Phys. Lett. **54**, 1760–1762 (1989).

[37] J. Pei, X. Gai, J. Yang, X. Wang, Z. Yu, D.-Y. Choi, B. Luther-Davies, and Y. Lu, Nat. Commun. **7**, 10450 (2016).

[38] N. J. Borys, E. S. Barnard, S. Gao, K. Yao, W. Bao, A. Buyanin, Y. Zhang, S. Tongay, C. Ko, J. Suh et al., ACS Nano **11**, 2115–2123 (2017).

[39] M.-A. Pinault and E. Tournié, Appl. Phys. Lett. **78**, 1562–1564 (2001).

[40] Q. Liang, J. Gou, Arramel, Q. Zhang, W. Zhang, and A. T. S. Wee, Nano Res. **13**, 3439–3444 (2020).

[41] S. Zhang, C.-G. Wang, M.-Y. Li, D. Huang, L.-J. Li, W. Ji, and S. Wu, Phys. Rev. Lett. **119**, 046101 (2017).

[42] F. Ali, F. Ahmed, M. Taqi, S. B. Mitta, T. D. Ngo, D. J. Eom, K. Watanabe, T. Taniguchi, H. Kim, E. Hwang, and W. J. Yoo, 2D Mater. **8**, 035027 (2021).

[43] Y. Liu, K. Tom, X. Zhang, S. Lou, Y. Liu, and J. Yao, New J. Phys. **19**, 073018 (2017).

[44] H. Shibata, Jpn. J. Appl. Phys. **37**, 550 (1998).

[45] S. Lin, B. Chen, W. Xiong, Y. Yang, H. He, and J. Luo, Opt. Express **20**, A706–A712 (2012).

[46] G.-H. Peng, P.-Y. Lo, W.-H. Li, Y.-C. Huang, Y.-H. Chen, C.-H. Lee, C.-K. Yang, and S.-J. Cheng, Nano Lett. **19**, 2299–2312 (2019).